Transactions on Engineering Sciences vol 9, © 1996 WIT Press, www.witpress.com, ISSN 1743-3533

Computation of the unsteady flow past a tuna with caudal fin oscillation

R. Ramamurti,[a] R. Löhner,[b] W. Sandberg[a]
[a]*Laboratory for Computational Physics and Fluid Dynamics, Naval Research Laboratory, Washington DC 20375, USA*
[b]*Institute for Computational Sciences and Informatics, The George Mason University, Fairfax, VA 22030, USA*

Introduction

The graceful motions of swimming fish, which appear almost effortless, have fascinated people for thousands of years, dating at least back to Aristotle, and possibly earlier, according to Lindsey [1]. In recent years, since the early 1970's, there has been increased experimental and analytical investigation of the physiology, biomechanics, and hydrodynamics of fish propulsion, for the purposes of quantifying the energy budget and actual swimming speeds for a variety of fish propulsive modes. These modes were classified by Breder [2] in 1926 and characterized steady forward swimming according to the occurrence and extent of body undulations, fin oscillations, and combinations of the two. For example the eel generates thrust via undulatory motion, while the tuna produces thrust almost exclusively through the oscillation of its lunate tail, or caudal fin. Webb [3,4], who has studied the morphologic adaptations of fish for optimized locomotion characterizes the tuna as a cruising specialist that has adapted for long distance steady swimming. Since the tuna body is relatively free from undulation it is an excellent case to examine analytically. The traditional hydrodynamics methods of slender body theory and elongated body theory unfortunately do not apply to the lunate fin of the tuna, as is discussed in detail by Yates [5], thus necessitating the use of unsteady lifting wing theories, which themselves require a number of simplifying assumptions to be made. Only recently has a capability for computing three-dimensional, unsteady incompressible flow over a changing geometry become available [6]. In that work, the flow field generated during a torpedo launch from a submarine was computed. In this paper we describe the extension of that work to carry out a direct computation, making no geometric simplifications, of the unsteady flow past the tuna, including the oscillatory caudal fin motion. In particular, we describe the computation of the time variation of the pressure distribution over the entire body and the integration over all surfaces to obtain the unsteady thrust. This is the first

such 3D incompressible flow, unsteady thrust computation for a deforming body that we are aware of.

The Incompressible Flow Solver

The governing equations employed are the incompressible Navier-Stokes equations in the arbitrary Lagrangian Eulerian (ALE) and can be written as

$$\frac{\partial \mathbf{v}}{\partial t} + \mathbf{v}_a \cdot \nabla \mathbf{v} + \nabla p = \nabla \cdot \sigma \ , \tag{1a}$$

$$\nabla \cdot \mathbf{v} = 0 \ , \tag{1b}$$

where p denotes the pressure, $\mathbf{v}_a = \mathbf{v} - \mathbf{w}$ the advective velocity vector (flow velocity $\mathbf{v}$ minus mesh velocity $\mathbf{w}$) and both the pressure p and the stress-tensor σ have been normalized by the (constant) density ρ, are discretized in time using an implicit timestepping procedure. It is important that the flow solver be able to capture the unsteadiness of a flow field if such exists. The present flow solver is built as time-accurate from the onset, allowing local timestepping as an option. The resulting expressions are subsequently discretized in space using a Galerkin procedure with linear tetrahedral elements. In order to be as fast as possible, the overhead in building element matrices, residual vectors, etc. should be kept to a minimum. This requirement is met by employing simple, low-order elements that have all the variables (u,v,w,p) at the same location. The resulting matrix systems are solved iteratively using a preconditioned gradient algorithm (PCG). The preconditioning is achieved through linelets [7]. The flow solver has been successfully evaluated for both 2-D and 3-D, laminar and turbulent flow problems by Ramamurti *et al.* [8,9]. The flow solver was also parallelized in order to improve its efficiency and portability to various supercomputer architectures. The parallelized grid generation and flow solver codes have been run on Intel iPSC/860, IBM SP-2 and CRAY C-90.

Rigid Body Motion

In order to fully couple the motion of rigid bodies with the hydrodynamic or aerodynamic forces exerted on them, consistent rigid body motion integrators must be developed. The governing equations of motion for rigid bodies can be found in textbooks on classical mechanics. The rigid body motion in 3-D is not straightforward due to its nonlinear character. The code integrates the pressure distribution on the surface to compute forces and moments at each time step and the equations of motion are advanced in time to produce self-consistent trajectories. A more detailed description of the equations and the incorporation of the rigid body motion in the numerical scheme for solving the fluid flow are described in [6].

Adaptive Remeshing

A fast regridding capability is essential for tracking important features in unsteady flows and the flow past deforming bodies. The surface motion and deformation of bodies may be severe, leading to distorted elements

which in turn lead to poor numerical results. If the bodies in the flow field undergo arbitrary movement, a fixed mesh structure will lead to badly distorted elements. This means that at least a partial regeneration of the computational domain is required. On the other hand, if the bodies move through the flow field, the positions of relevant flow features will change. Therefore, in most of the computational domain a new mesh distribution will be required. One approach to solve these problems is to regenerate the whole computational domain adaptively, taking into consideration the current flow field solution. A typical simulation where bodies undergo severe motion typically requires hundreds of remeshings. Therefore, the grid generator must be reliable and fast. In order to generate or regenerate a mesh reliably and quickly, we use the advancing front technique [10,11].

We have also recently increased the reliability of the grid generator to a point where it can be applied on a routine basis in a production environment. This significant increase in reliability was achieved by skipping those faces that do not give rise to good elements. If pockets of unmeshed regions remain, we enlarge them somewhat, and regrid them. This 'sweep and retry' technique has proven extremely robust and reliable.

The use of optimal data structures, filtering of points and faces and automatic reduction of unused points along the advancing front has increased the speed of the grid generation process [6]. Currently, the advancing front algorithm constructs grids at a rate of 60,000 for very small grids to 80,000 tetrahedra per minute for large grids on the CRAY-C90.

Practical simulations revealed that the appearance of badly distorted elements occurred more often than expected. Given the relatively high cost of global remeshing, we explored the idea of local remeshing in the vicinity of the elements that became too distorted. Here, the badly distorted elements and the elements that surround it are removed. Then, a new mesh is generated in the holes left by the removal of these elements. This is a fast process and takes 5-6 times less CPU time compared to global remeshing.

The identification of the region of moving elements and the mesh movement algorithm to be employed are also important from the point of view of mesh distortion and remeshing requirements. These are discussed in detail in [6].

Numerical Examples

2-D Undulating Eel

In order to observe the process of longitudinal force generation by body undulation, a 2-D simulation of a swimming eel was considered first. The computation was performed primarily to test the coupled rigid body motion with the adaptive remeshing flow solver. Therefore, the parameters chosen for the body undulation may not represent actual eel motion. The body undulation was prescribed as a sinusoidal wave traveling from the head to tail as follows:

$$y = Asin\left\{2\pi(tf - \frac{x}{\lambda})\right\} \tag{2a}$$

The amplitude A is given by

$$A = \begin{cases} 0, & x < x_0, \\ A_{max}\ B(x), & x_0 < x < x_1 \text{ and} \\ A_{max}, & x > x_1. \end{cases} \tag{2b}$$

where A_{max} is the maximum amplitude, $B(x)$ is a blending function in the region x_0 to x_1, t is the time, f is the frequency and λ is the wavelength of the traveling wave.

Several computations were performed by varying the traveling wave-speed and the amplitude of the wave. The computational grid, Fig. 1, shows adaptation to the body motion where 8 layers of elements that surround the eel move with it rigidly. In all the cases studied, the frequency f was maintained to be 1.5 Hz.

Case 1: The first simulation was performed with $\lambda = 1.0\ L$, $A_{max} = 0.1\ L$, where L is the length of the eel. The variation of the thrust and the side force with time is shown in Fig. 2a. The mean thrust in this case is 0.0495 directed towards the head.

Case 2: Next, the wavelength of the traveling wave λ was decreased to 0.5 L. The variation of the force components are shown in Fig. 2b. The mean thrust in this case is 0.047 directed towards the tail. This is due to the cancellation of the pressure force in the region of the tail which is responsible for a major contribution to the thrust.

Case 3: As λ is increased to 1.25 the mean thrust increased to 0.0817 directed towards the head.

Case 4: Finally, the maximum amplitude, A_{max}, was increased to 0.2 L. In this case, the mean thrust increased to 0.33 directed toward the head.

3-D Steady Flow Past a Tuna

Next the three-dimensional flow past a tuna with an oscillating caudal fin was simulated. The motion of the caudal fin was prescribed as follows

$$z = A \sin(\omega t) \frac{(x - x_0)^2}{(x_1 - x_0)^2}, \tag{3}$$

where A is the amplitude of the motion at the tip of the caudal fin, ω is the angular frequency, x_0 is the location of the peduncle, which is the smallest part of the body where the caudal fin begins, and x_1 is the location of the tip of the caudal fin. The mean line is prescribed as a parabolic arc from the peduncle so as to maintain C_1 (slope) continuity throughout the entire body. This also implies that the caudal fin must deform during the motion.

Several steady state solutions were obtained at various caudal positions during one quarter of a cycle. Forces generated by the caudal fin and the body were computed. Unsteady flow was computed for 3 cycles and the results compared with the steady-state one quarter cycle data.

3-D Unsteady Flow Past a Tuna

In order to demonstrate the capability of the newly developed flow solver to compute flow past deformable bodies and to study trends, we first approximated the high Reynolds-number flow by an inviscid flow. An inviscid flow will require a much coarser grid, which translates to fast turnaround.

The speed of the tuna was set to 10 $L/sec.$ [3]. First a steady state solution was obtained. With this flow field as the initial condition, the unsteady flow for 3 cycles of the caudal fin oscillation was computed. The time step $\Delta t = 10^{-4}$ was employed and the entire unsteady computation was performed in 2400 steps. During this interval, 161 local remeshings and 1 global remeshing were carried out. The grid for this computation consisted of approximately 52K points and 262K tetrahedra. The total computational time for this computation is approximately 12 CPU hours on a CRAY C-90. The time taken for advancing the flow 1 timestep is 17 sec. per point, the time for 1 local remeshing is 38 secs. and the time for 1 global remesh is 300 secs.

The time variation of the force components for the first 3 cycles is shown in Fig. 3. This shows that the thrust developed by the caudal fin motion is not quite sufficient to balance the nearly constant drag on the body. Figure 4 shows the effect of the caudal fin position on the force components, both for the steady and unsteady simulations. It is clear that the steady state simulation can capture neither the magnitude nor the trend of the variation of the forces seen in the unsteady simulation results. Figures 5 shows the differences in the surface pressure distribution between the steady state and unsteady computation on the pressure and suction sides of the caudal fin. The minimum pressure in the unsteady computation is lower compared to the steady state computation. The maximum pressure which occurs at the leading edge of the fin remains almost unchanged. In the steady state computations, Figs. 5a and 5c, the pressure contours are symmetric about the 'centerline' of the fish whereas the unsteady computations result in a higher pressure on the lower side of the peduncle. Figure 6 shows the surface pressure distribution at the end of 3 cycles. The high pressure regions in this case are near the mouth, the leading edges of the fins and near the gill. The velocity vectors on the surface, Fig. 7, show a low velocity region extending from the mouth to the tail along the centerline. We believe this is due to the open mouth geometry. Since the fish mouth is not always open the low velocity regime does not persist but is rather more intermittent. This conjecture requires further examination. A small recirculation region is also evidenced near the peduncle region. This is due to the corner flow that is set up at the maximum amplitude of oscillation. Triantafyllou *et al.* [12] have carried out investigations of the experimental flow past a robotic tuna. Future plans include Navier-Stokes computations for comparison with this data.

Conclusions

A new, 3-D incompressible flow solver based on simple finite elements with adaptive remeshing has been developed and validated. The main algorithmic ingredients were described in this paper and some validation results shown. We have demonstrated how the combination of adaptive remeshing techniques, flow solvers for transient problems with moving grids, and integrators for rigid body motion allows the simulation of fully coupled fluid-rigid body interaction problems of arbitrary geometric complexity in three dimensions. Areas that deserve further study are the diffusive effect of interpolation while remeshing and extension to Navier-Stokes problems.

Acknowledgments

This work was supported by the Laboratory for Computational Physics and Fluid Dynamics of the Naval Research Laboratory.

References

1. Lindsey, C.C., "Locomotion," in *Fish Physiology*, **7**, ed. W.S. Hoar and D.J. Randall, Academic Press, 1978.
2. Breder, C.M., "The Locomotion of Fishes," *Zoologica*, **4**, pp. 159-256, N.Y., 1926.
3. Webb, P.W., "Form and Function in Fish Swimming," *Scientific American*, **251**, (1), 72, 1984.
4. Weihs, D. and Webb, P.W., "Optimization of Locomotion," in *Fish Biomechanics*, ed. P.W. Webb and D. Weihs, Praeger Scientific, 1983.
5. Yates, P.W., "Hydromechanics of Body and Caudal Fin Propulsion," in *Fish Biomechanics*, *ibid.*
6. R. Ramamurti, R. Löhner and W.C. Sandberg, "Simulation of a Torpedo Launch Using a 3-D Incompressible Finite Element Solver," *AIAA-95-0086*, Washington, D.C., 1995.
7. Martin, D. and Löhner, R., "An Implicit Linelet-Based Solver for Incompressible Flows," *AIAA*-92-0668, Washington, D.C., 1992.
8. Ramamurti, R. and Löhner, R., "Evaluation of an Incompressible Flow Solver Based on Simple Elements," *Advances in Finite Element Analysis in Fluid Dynamics*, FED Vol. 137, Editors: M.N. Dhaubhadel et al., ASME Publication, New York, pp. 33-42, 1992.
9. R. Ramamurti, R. Löhner and W.C. Sandberg, "Evaluation of a Scalable 3-D Incompressible Finite Element Solver," *AIAA-94-0756*, Washington, D.C., 1994.
10. R. Löhner and P. Parikh, "Three-Dimensional Grid Generation by the Advancing Front Method," *Int. J. Num. Meth. Fluids* 8, pp. 1135-1149, 1988.
11. J. Peraire, K. Morgan and J. Peiro, " Unstructured Finite Element Mesh Generation and Adaptive Procedures for CFD," AGARD-CP-464, 18, 1990.
12. M. S. Triantafyllou and G. S. Triantafyllou, "An Effiecient Swimming Machine," *Scientific American*, pp. 64-70, March 1995.

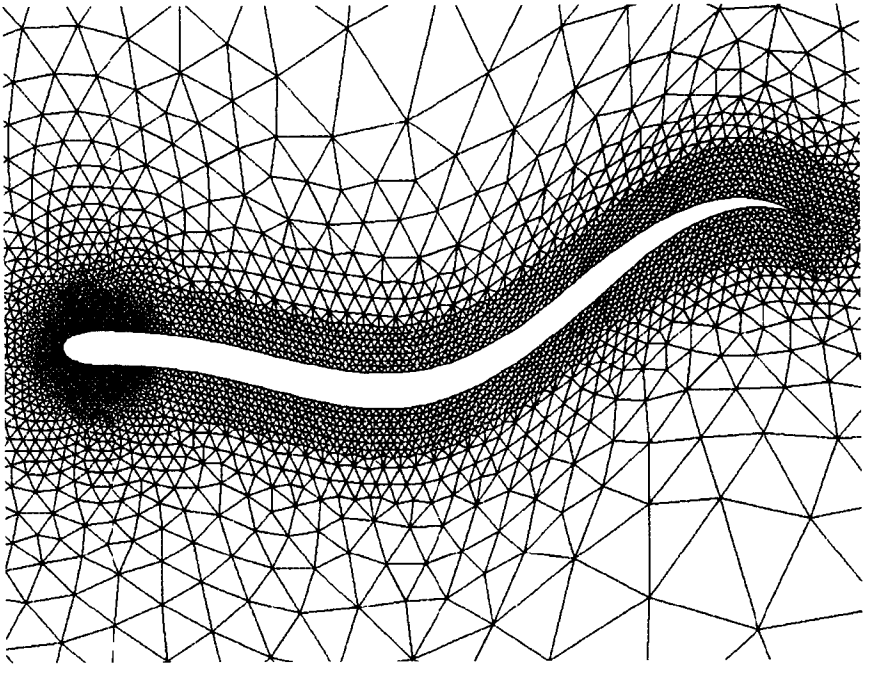

Fig. 1. Adapted Mesh About an Undulating Eel, nelem= 9,792, npoin= 5,091

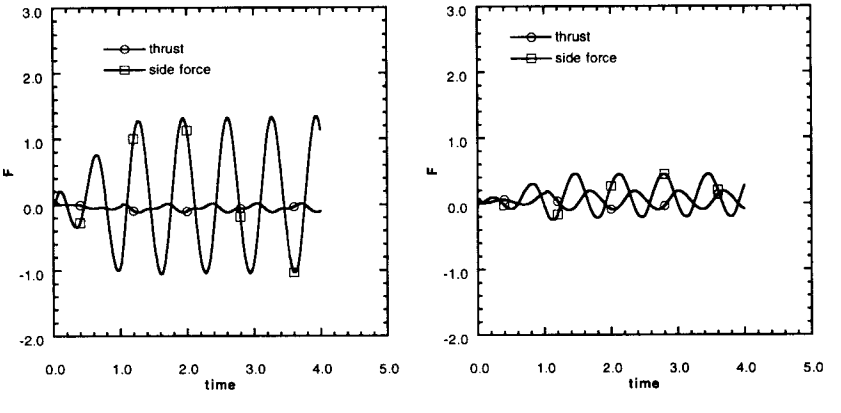

a. $\lambda = 1.0\ L, A_{max} = 0.1$ **b.** $\lambda = 0.5\ L, A_{max} = 0.1$

Fig. 2. Time History of Force on an Undulating Eel

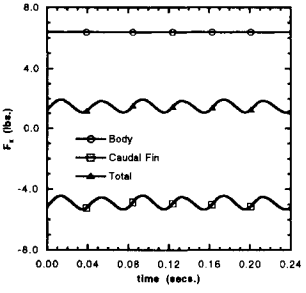

a. x-component

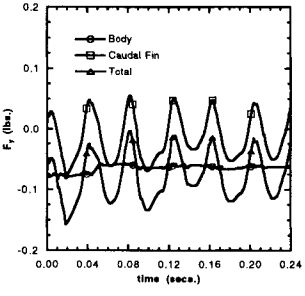

b. y-component

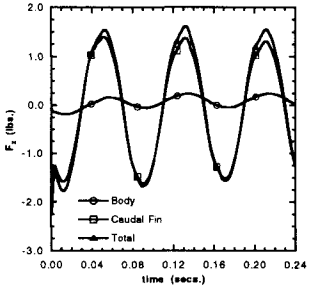

c. z-component

Fig. 3. Time Variation of Force on a Swimming Tuna

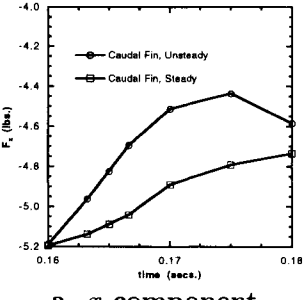

a. x-component

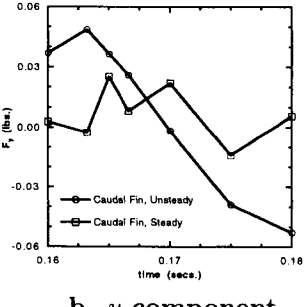

b. y-component

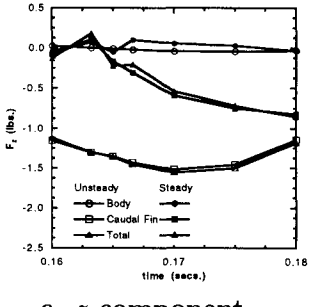

c. z-component

Fig. 4. Effect of Caudal Fin Position on Forces

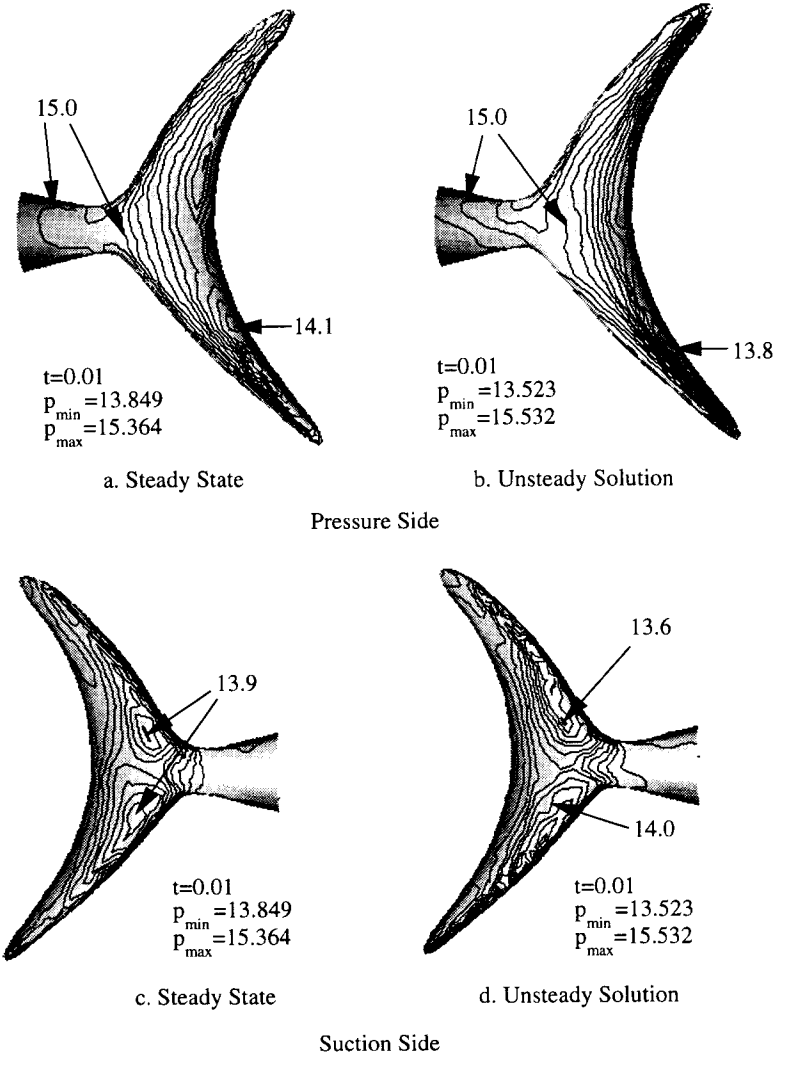

a. Steady State

b. Unsteady Solution

Pressure Side

c. Steady State

d. Unsteady Solution

Suction Side

Fig. 5. Comparison of Pressure Distribution on the Caudal Fin

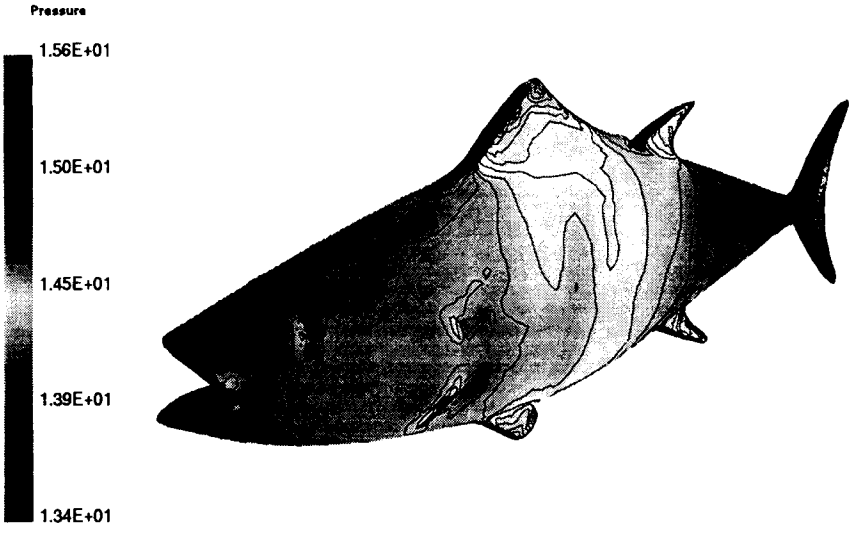

Fig. 6. Surface Pressure Distribution on a Swimming Tuna, t=0.24 Secs.

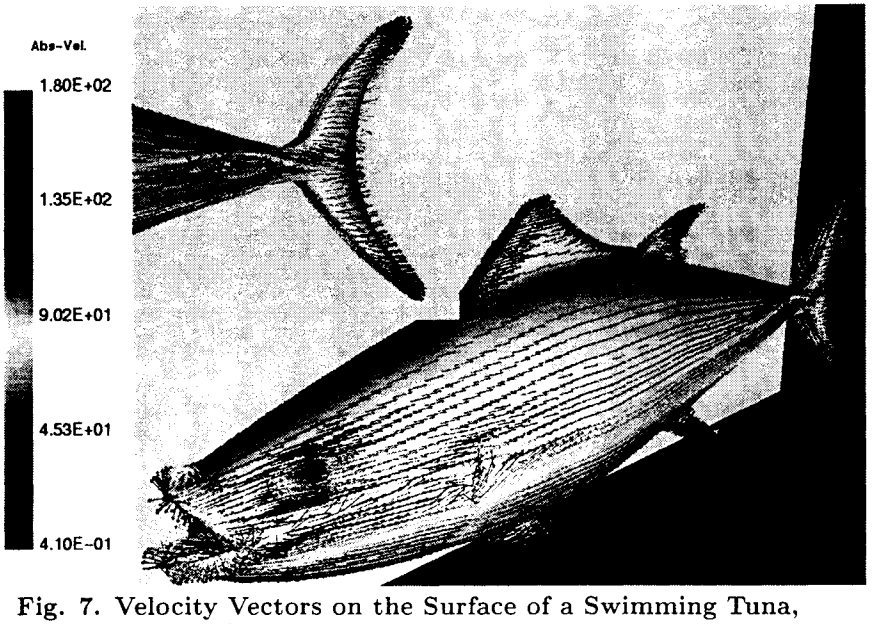

Fig. 7. Velocity Vectors on the Surface of a Swimming Tuna, t=0.24 Secs.